Designer Crystals: Single Crystals with Complex Morphologies

Barbara Wucher, Wenbo Yue, Alex N. Kulak, and Fiona C. Meldrum*

School of Chemistry, University of Bristol, Cantock's Close, Bristol BS8 1TS, United Kingdom

Received August 31, 2006. Revised Manuscript Received December 24, 2006

Biological systems are capable of remarkable control over crystal growth, producing morphologically complex single crystals with curved surfaces. We have previously demonstrated that crystals with identical morphological complexities can be produced synthetically using templating routes. This article provides a detailed investigation into the mechanism of this process, studying the relationship between the chemical environment provided by the template and the structure of the templated particles produced. A range of crystals were precipitated within the confines of macroporous polymer templates whose surface chemistries were varied by oxidation with an oxygen plasma, by modification with adsorbed polyelectrolytes, or by electroless deposition of a thin layer of gold and subsequent functionalization with ω-terminated self-assembled monolayers. The surface chemistry of the template was shown to play a crucial role in determining the structure of templated calcite particles, such that only non-charged surfaces directed the formation of single-crystal particles and polycrystalline particles being produced with negatively charged surfaces. Control of crystal morphologies is clearly fundamental to the development of many new functional materials and devices. This work therefore demonstrates how a templating methodology can provide a general and highly controllable route to synthesizing crystalline materials with defined morphologies and structures.

Introduction

The remarkable and frequently complex morphologies displayed by many biominerals offer a unique inspiration for materials design.[1,2] Structural examination of these biogenic minerals reveals that many of those with the most exotic morphologies, such as silicaceous diatoms and radiolaria, are constructed from amorphous minerals.[3,4] With no preferred form, an amorphous material can be readily molded to give any selected product shape and thus appears to be the automatic choice for construction of an elaborate structure.[5] Polycrystalline biominerals also exhibit a wide range of morphologies, and it is again intuitive that small crystalline building blocks can be organized to give complex forms. Perhaps the most remarkable category of biominerals, however, is the single crystals with complex form. Under equilibrium conditions, crystals grow to produce regular, geometric morphologies which reflect the symmetry of the internal crystal lattice.[6] Biological control, in contrast, can yield single crystals whose external form bears no relation to the crystallographic structure. A perfect example is offered by the skeletal plates of sea urchins, each of which exhibits a bicontinuous, sponge-like structure and curved surfaces and yet is a single crystal of calcite.[7−9]

This paper will focus on the formation of single crystals with complex morphologies. Control of crystal morphologies is fundamental to many applications, ranging from the preparation of homogeneous populations of particles for use as coatings and pigments to the development of new functional materials and devices. Further, single crystals can exhibit superior optical and electronic properties as compared with their polycrystalline counterparts. A beautiful example is found in biology, where certain skeletal plates of light-sensitive brittle stars, which are formed from single crystals of calcite, are structured to act as lenses, focusing light onto sensors within the organism.[10] A range of mechanisms are believed to operate in vivo to modify crystal morphologies.[2,6,11] As soluble additives, the macromolecules extracted from a number of calcite biominerals have been shown to interact with specific crystal planes during $CaCO_3$ re-growth experiments, producing relatively minor adaptations in crystal morphologies.[12,13] Complex single-crystal morphologies, such as the sponge-like form of the skeletal elements of echinoderms or the hammerhead-shaped single-crystal elements of the coccolith *Emiliania Huxleyi* are characteristic of crystallization within structured vesicles, where the morphology of the vesicle dictates the gross form of the crystal growing within it.[9,14] Changes in the activity or positioning of ion

* To whom correspondence should be addressed. E-mail: Fiona.Meldrum@bristol.ac.uk.

(1) Thompson, D. A. *On Growth and Form*; Cambridge University Press: Cambridge, 2004.
(2) Lowenstam, H. A.; Weiner, S. *On Biomineralization*; Oxford University Press: New York, 1989.
(3) Bauerlein, E. *Angew. Chem., Int. Ed.* **2003**, *42*, 614−641.
(4) Muller, W. E. G., Ed. *Silicon Biomineralization*; Springer-Verlag: Berlin, 2003; Vol. 33.
(5) Weiner, S.; Addadi, L. *J. Mater. Chem.* **1997**, *7*, 689−702.
(6) Meldrum, F. C. *Int. Mater. Rev.* **2003**, *48*, 187−224.
(7) Smith, A. B. *Spec. Pap. Paleontol.* **1980**, *25*, 1−81.
(8) Donnay, G.; Pawson, D. L. *Science* **1969**, *166*, 1147.
(9) Dubois, P.; Chen, C. P. In *Echinoderm Studies*; Jangoux, M., Lawrence, J., Eds.; AA Balkema: Rotterdam, 1989; Vol. 3, pp 109−178.
(10) Aizenberg, J.; Tkachenko, A.; Weiner, S.; Addadi, L.; Hendler, G. *Nature* **2001**, 412, 819−822.
(11) Mann, S. *Biomineralization: Principles and Concepts in Bioinorganic Materials Chemistry*; Oxford University Press: New York, 2001.
(12) Albeck, S.; Addadi, L.; Weiner, S. *Connect. Tissue Res.* **1996**, *35*, 365−370.
(13) Albeck, S.; Aizenberg, J.; Addadi, L.; Weiner, S. *J. Am. Chem. Soc.* **1993**, *115*, 11691−11697.

10.1021/cm0620640 CCC: $37.00
Published on Web 02/09/2007

pumps and channels during mineralization may also lead to crystal growth in preferred directions.[11]

Morphological control of single crystals in synthetic systems is often carried out to produce a homogeneous population of particles for applications such as coatings and fillers and is typically achieved through the use of either organic or inorganic additives.[15−18] In common with the biological strategy, templating routes have been applied to produce more elaborate morphologies. Using amorphous calcium carbonate (ACC) as a precursor phase, Loste et al. produced rod-shaped single crystals of calcite within the confines of track-etch membrane pores,[19,20] while Aizenberg et al. synthesized perforated calcite single crystals within a mold comprising a regular array of pillars via an ACC precursor phase.[21] In previous work we have also shown that single crystals of calcite with complex morphologies can be synthesized by direct mixing of Ca^{2+} and CO_3^{2-} ions in a suitable template under double diffusion conditions.[22,23] Precipitation within the confines of a sponge-like polymer membrane, formed as a replica of sea urchin skeletal plates, yielded single crystals of calcite with morphologies identical to that of the original urchin plate. This was achieved in the absence of organic additives, indicating that control of crystal morphologies to produce elaborate shapes and curved surfaces can be achieved by shape constraint only. Extension to a wide range of other minerals including $SrSO_4$, $PbSO_4$, NaCl, and $CuSO_4$ further demonstrated the generality of this templating approach.[24]

It is clear, however, that to produce single crystals of unusual morphology control must be exerted not only during growth but also at the point of nucleation. While a high density of nuclei will develop into a polycrystalline product, a single crystal must necessarily derive from a single nucleation site. Crystal nucleation in biological systems often occurs in association with insoluble organic matrices, which can mediate the formation of highly oriented crystallites in a well-defined spatial distribution.[2,11] This process has been modeled using model organic membranes including Langmuir monolayers,[25−28] Langmuir−Blodgett films,[29] and self-assembled monolayers (SAMs).[30−32] The mechanism by which orientational information is translated from an organic matrix to the developing crystallite is frequently debated, with the traditional theory arguing epitaxial control.[33] Recent experiments have suggested that orientational control can be determined by the average charge density at the organic matrix[27] and the orientation of the monolayer headgroups,[30,32] and it has been demonstrated that the highly oriented aragonite tablets comprising mollusk shell nacre actually grow within a gel-like environment, requiring a reconsideration of the long-held epitaxial model of orientational control.[34] An increasing body of evidence also suggests that calcification in organisms frequently proceeds via a transient ACC phase,[35−39] which may again require a re-evaluation of currently held mechanisms of orientational control.[34]

The work described in this paper investigates the mechanism of formation of single crystals with complex morphologies via templating routes, thereby demonstrating how the experimental method can be tailored to produce crystalline particles with controlled morphologies and crystalline structures. Specifically, we investigate how the chemical environment generated by the template, as defined by its surface chemistry, can be chosen to generate either single crystal or polycrystalline particles, as desired. The experiments develop from our previous studies and use polymer membranes, formed as replicas of sea urchin skeletal plates, as templates to form particles with complex, sponge-like forms. The generality of the approach was investigated by studying the growth of $CaCO_3$ (calcite), $SrSO_4$, and $PbSO_4$ crystals within the surface-treated membranes, all of which had been previously demonstrated to support the formation of templated single crystals within the untreated polymer membranes.[24] We therefore show that crystallization within a suitable constrained environment provides a very flexible and controllable route to the production of particles with selected morphologies and structures.

Experimental Section

Crystallization of $CaCO_3$, $SrSO_4$, and $PbSO_4$ was carried out within structured polymer membranes, formed as replicas of sea urchin skeletal plates, as described below. The surface chemistries of these polymer templates were modified prior to use in the

(14) Young, J. R.; Henriksen, K. In *Biomineralization*; Weiner, S., Dove, P., Eds.; Mineralogical Society of America: Washington, DC, 2003; Vol. 54, pp 189−215.
(15) Yu, S. H.; Colfen, H. *J. Mater. Chem.* **2004**, *14*, 2124−2147.
(16) Mukkamala, S. B.; Powell, A. K. *Chem. Commun.* **2004**, 918−919.
(17) Mann, S.; Didymus, J. M.; Sanderson, N. P.; Heywood, B. R.; Samper, E. J. A. *J. Chem. Soc., Faraday Trans.* **1990**, *86*, 1873−1880.
(18) Kuther, J.; Seshadri, R.; Tremel, W. *Angew. Chem., Int. Ed.* **1998**, *37*, 3044−3047.
(19) Loste, E.; Park, R. J.; Warren, J.; Meldrum, F. C. *Adv Funct. Mater.* **2004**, *14*, 1211−1220.
(20) Loste, E.; Meldrum, F. C. *Chem. Commun.* **2001**, *10*, 901−902.
(21) Aizenberg, J.; Muller, D. A.; Grazul, J. L.; Hamann, D. R. *Science* **2003**, *299*, 1205−1208.
(22) Park, R. J.; Meldrum, F. C. *J. Mater. Chem.* **2004**, *14*, 2291−2296.
(23) Park, R. J.; Meldrum, F. C. *Adv. Mater.* **2002**, *14*, 1167−1169.
(24) Yue, W.; Kulak, A. N.; Meldrum, F. C. *J. Mater. Chem.* **2006**, *16*, 408−416.
(25) Heywood, B. R.; Mann, S. *Adv. Mater.* **1994**, *6*, 9−20.
(26) Berman, A.; Ahn, D. J.; Lio, A.; Salmeron, M.; Reichert, A.; Charych, D. *Science* **1995**, *269*, 515−518.
(27) Volkmer, D.; Fricke, M.; Gleiche, M.; Chi, L. F. *Mater. Sci. Eng. C* **2005**, *25*, 161−167.
(28) Cavalli, S.; Popescu, D. C.; Tellers, E. E.; Vos, M. R. J.; Pichon, B. P.; Overhand, M.; Rapaport, H.; Sommerdijk, N. A. J. M.; Kros, A. *Angew. Chem., Int. Ed.* **2006**, *45*, 739−744.
(29) Hughes, N. P.; Heard, D.; Perry, C. C.; Williams, R. J. P. *J. Phys D: Appl. Phys.* **1991**, *24*, 146−153.
(30) Aizenberg, J.; Black, A. J.; Whitesides, G. M. *J. Am. Chem. Soc.* **1999**, *121*, 4500−4509.
(31) Aizenberg, J.; Black, A. J.; Whitesides, G. M. *Nature* **1999**, *398*, 495−498.
(32) Travaille, A. M.; Kaptijn, L.; Verwer, P.; Hulsken, B.; Elemans, J. A. A. W.; Nolte, R. J. M.; van-Kempen, H. *J. Am. Chem. Soc.* **2003**, *125*, 11571−11577.
(33) Weiner, S.; Traub, W. *Philos. Trans. R. Soc. London, Ser. B* **1984**, *304*, 421−438.
(34) Addadi, L.; Joester, D.; Nudelman, F.; Weiner, S. *Chem.−Eur. J.* **2006**, *12*, 981−987.
(35) Beniash, E.; Addadi, L.; Weiner, S. *J. Struct. Biol.* **1999**, *125*, 50−62.
(36) Beniash, E.; Aizenberg, J.; Addadi, L.; Weiner, S. *Proc. R. Soc. London, Ser. B* **1997**, *264*, 461−465.
(37) Weiss, I. M.; Tuross, N.; Addadi, L.; Weiner, S. *J. Exp. Zool. B* **2002**, *293*, 478−491.
(38) Nassif, N.; Pinna, N.; Gehrke, N.; Antonietti, M.; Jager, C.; Colfen, H. *Proc. Natl. Acad. Sci. U.S.A.* **2005**, *102*, 12653−12655.
(39) Politi, Y.; Levi-Kalisman, Y.; Raz, S.; Wilt, F.; Addadi, L.; Weiner, S.; Sagi, I. *Adv. Funct. Mater.* **2006**, *16*, 1289−1298.

expectation of generating surfaces which would vary in their ability to influence crystal nucleation and, therefore, the product particle structure, via treatment either with an oxygen plasma followed by adsorption of charged polyelectrolytes or with electroless deposition of Au, followed by functionalization with SAMs.

Preparation of Polymer Membrane Replicas of Sea Urchin Skeletal Plates. A method identical to that described previously was used.[24] Briefly, a clean sea urchin test was separated into individual skeletal plates, which were then washed by sonication in ethanol and dried at 60 °C prior to use. A plate was then immersed in a polymer monomer solution comprising 7:13 (v/v) ethyl acrylate to methyl methacrylate and 0.5% (w/v) benzoyl peroxide as initiator. This system was placed under vacuum to remove air from the sea urchin plate and ensure complete infiltration. Finally, the monomer solution containing the urchin plate was heated under argon at 65 °C for ~48 h until polymerization was complete. Membranes were then produced by cutting sections of thickness ~ 0.5 mm through the polymer-infiltrated urchin plate using a hand-operated microtome fitted with a steel blade. Finally, the $CaCO_3$ was removed from the cut sections by immersion in hydrochloric acid (37%) for 30 min, decanting the acid, and repeating the dissolution process twice more. The polymer membranes were finally washed with copious quantities of Milli-Q water and were dried in vacuum.

Surface Treatment of Polymer Membranes. Three methods were investigated for modification of the surfaces of the polymer membranes. (1) A thin layer of gold was deposited on the membrane surface using electroless deposition according to the procedure described by Menon and Martin,[40] followed by modification with ω-functionalized SAMs. (2) The surface of the polymer membrane was rendered more hydrophilic by treatment with an oxygen plasma. (3) Positively charged polyelectrolytes were adsorbed onto oxygen-plasma-treated membranes to give positively charged membrane surfaces.

(1) Electroless Deposition of Gold and Modification with SAMs. A membrane was initially immersed in a tin-containing solution comprising 0.026 M $SnCl_2$ and 0.07 M trifluoroacetic acid in a solvent of 1:1 methanol/water for 3 min, and a vacuum was applied to ensure complete infiltration of the solution into the membrane pores. The membrane was then washed three times with Milli-Q water to remove unbound Sn^{2+} ions. The Sn^{2+}-sensitized membrane was then immersed in a 0.029 M solution of ammoniacal $AgNO_3$ for 2 min, again under vacuum, and was then washed two times with methanol. This process causes a redox reaction in which the surface-bound Sn(II) was oxidized to Sn(IV) and the Ag^+ was reduced to elemental Ag. Finally, gold coating of the membrane was achieved by placing a silver-coated membrane in a solution containing 7.9 mM $Na_3Au(SO_3)_2$ (prepared by dilution from Oromerse Part B, Technic, Inc., U.S.A., a commercially available gold electroless deposition solution), 0.127 M Na_2SO_3, and 0.025 M $NaHCO_3$ in 1:1 formaldehyde/water at 0−2 °C for 90 min under vacuum. The silver particles are galvanically displaced by the more noble gold during this process. After removal from solution the membrane was washed thoroughly with water and was then placed in 25% nitric acid for at least 12 h to remove any residual tin or silver. The membranes were again washed thoroughly after this procedure and were dried with compressed air.

The surface chemistry of the gold-coated membranes was then systematically modified using SAMs. The coated membranes were immersed in 10 mM ethanolic solutions of the ω-functionalized thiols 16-mercaptohexadecanoic acid, 1-hexadecanethiol, 3-mercapto-1-propanesulfonic acid sodium salt, 4-mercaptophenol, and 3-mercapto-1-propanol for ~24 h (all thiols were obtained from Aldrich and used as received), followed by rinsing with ethanol and drying with compressed air.

(2) Oxygen-Plasma Treatment. The prepared polymer membranes were placed in a Harrick Plasma PDC-32G plasma cleaner and were exposed to an oxygen plasma for 5 min. The membranes were then used immediately for crystal growth experiments.

(3) Polyelectrolyte Treatment. The polymer membranes were rendered negatively charged using oxygen-plasma treatment as described in section 2. These membranes were then immersed in a 1% aqueous solution of poly(ethylene imine) (Alfa Aesar, branched, molecular weight 10 000) for 15 min, prior to washing with copious quantities of water to give the membrane an overall positive charge.

Precipitation of Crystals within Surface-Treated Polymer Membranes. Crystals of $CaCO_3$, $SrSO_4$, and $PbSO_4$ were precipitated within the urchin membranes using a double diffusion technique from solutions of $CaCl_2$ and Na_2CO_3, $SrCl_2$ and Na_2SO_4, and $Pb(NO_3)_2$ and $Na_2(SO_4)$, respectively.[24] The pH values of the solutions were measured prior to use and corrected as required using NaOH solution. Membranes were immersed in water and placed under vacuum to ensure complete infiltration of the solution into the membrane pores and were then mounted between two U-tube arms. Equal volumes of solutions of identical concentration and solutions of the selected cations and anions were then simultaneously injected into the U-tube arms, and crystallization was typically allowed to proceed for 24 h.

Isolation of Crystals from Polymer Membranes. After completion of the crystallization experiment, the membrane was removed from the U-tube setup, was washed with water, and was dried with compressed air. The membrane was then dissolved in chloroform, the crystals were allowed to settle, and the solvent was decanted. This procedure was repeated many times to ensure that all residual polymer had been removed from the crystals. The crystals were then transferred to a glass coverslip for examination in the scanning electron microscope.

Analysis of Crystals Precipitated within Membranes. The morphologies of the crystals precipitated within the membranes were investigated using scanning electron microscopy (SEM). Glass slides supporting the crystals for analysis were mounted on SEM stubs with adhesive carbon pads and were sputter coated with Pt/Pd using an Agar high-resolution sputter coater. SEM was carried out using either a JEOL JSM 5600LV or a JEOL JSM 6330F scanning electron microscope, operating at 15 keV. Energy-dispersive X-ray analysis (EDXA) was performed using an Oxford Instruments ISIS 300 system with silicon detector, and high-resolution elemental distribution maps were prepared of the Au-coated membranes to demonstrate uniform distribution of the Au throughout the membrane.

Selected crystals were also examined using single-crystal X-ray diffraction (XRD) to investigate their single-crystal/polycrystalline structure. Suitable crystals for single-crystal XRD were located by optical microscopy and were mounted on a glass fiber of 1.5−2.0 mm in length using hydrocarbon or silicone grease. Single-crystal X-ray diffraction measurements were recorded using a Smart or Proteum single-crystal X-ray diffractometer with Cu Kα radiation.

Analysis of Calcium Carbonate Precipitated within Membranes at Early Times. Early stages of $CaCO_3$ precipitation in the membranes were investigated by removal of membranes from the double diffusion setup after 15 min and then washing with water and ethanol. The morphologies of the particles precipitated within this time frame were determined using SEM following the sample preparation method outlined above. Identification of the $CaCO_3$ polymorphs produced was carried out using Raman microscopy of the particles in situ in the dried membrane with a Renishaw inVia

(40) Menon, V. P.; Martin, C. R. *Anal. Chem.* **1995**, *67*, 1920−1928.

Raman microscope, operating with a LaserPhysics 488 nm Ar-ion laser at 20 mW.

Analysis of Surface-Treated Polymer Using Contact Angle Measurements. The surface treatments of the polymers were investigated using contact angle measurements. To avoid complications in the analysis arising from the porous structure of the membranes, nonporous ethyl acrylate/methyl methacrylate polymers were synthesized using the same monomer concentrations and experimental conditions as applied previously for preparation of the urchin polymer membranes. Sections of ~1 mm thick were cut through the uniform cured polymer using a hand-operated microtome, and the polymer slices were surface-treated using identical procedures as described for the porous polymer membranes, with the exception that immersion in the thiol solutions was carried out for 1 h only, as a result of some lift-off of the Au film from the polymer with long incubation times. Advancing and receding contact angle measurements were made on freshly prepared samples using a drop shape analysis system (G10/DSA10 Krüss).

Results

Surface Treatment of Polymer Membranes. The gold-coating procedure adopted effectively produced a uniform coverage of gold particles on the surface of the polymer membrane, resulting in a membrane which was dark purple in color. An incubation time of 90 min in the gold deposition solution was found to be optimal as this produced a uniform thin film of gold on the polymer surface but did not block the membrane surface pores as occurred when thicker, gold-colored films were deposited at longer incubation times. Uniform coverage of the membrane with gold particles after 90 min was confirmed through SEM analysis of a cross section taken through the center of the membrane (Figure 1a) and through recording a Au elemental distribution map of the same area (Figure 1b). EDXA analysis of the polymer also confirmed complete removal of the Sn and Ag present during the electroless deposition process. Examination of the Au-coated membrane at higher magnifications showed that the Au film comprised a densely packed film of gold particles 50−100 nm in size, with the presence of a small number of larger aggregates of particles.

The surface chemistry of these gold films was then determined by deposition of SAMs of ω-functionalized thiols. The effect of these surface treatments was evaluated through contact angle measurements and compared with the unmodified polymer surface, a gold-coated polymer surface, and an oxygen-plasma-treated polymer surface. The advancing and receding contact angles measured (taken as an average of three measurements) are shown in Table 1. The relatively large hysterisis between the advancing and receding angle reflects the high roughness of the polymer surfaces. The measurements show that functionalization of the polymer surface with Au SAMs has little effect on the hydrophilicity of the surface, with the exception of the methyl-terminated hexadecanethiol which clearly renders the surface more hydrophobic. The oxygen-plasma treatment is also effective in increasing the wettability of the polymer surface.

Crystal Growth in Polymer Membranes. $CaCO_3$ was precipitated within the untreated and surface-treated membranes from 0.02 M $CaCl_2$ and 0.02 M Na_2CO_3 solutions. The untreated membranes yielded ~ 100 μm single crystals of calcite, with sponge-like morphologies and curved surfaces

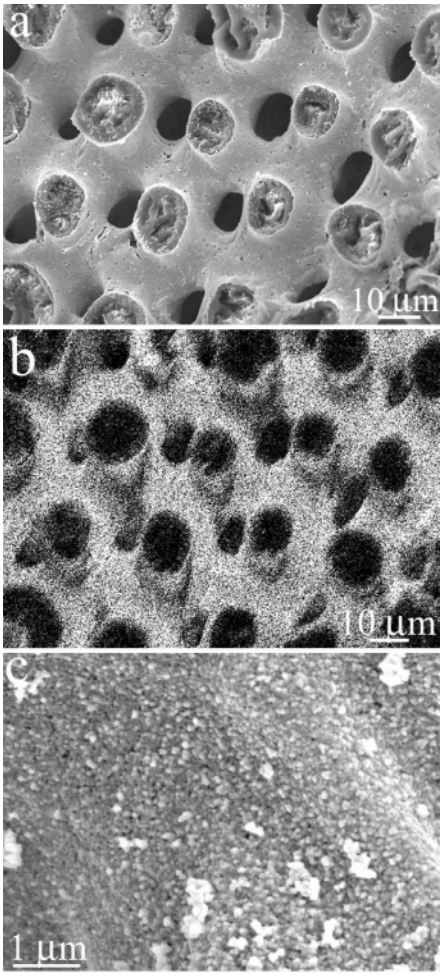

Figure 1. SEM images of (a) a cross section through a gold-coated polymer membrane and (b) a gold elemental distribution map taken of the same area. (c) A high magnification image showing a uniform distribution of gold particles on the membrane surface.

Table 1. Advancing and Receding Contact Angle Measurements Recorded for the Polymer and Surface-Modified Polymers

membrane	advancing angle (deg)	receding angle (deg)
untreated	75	30
oxygen plasma treated	46	10
gold coated	68	13
gold/mercaptohexadecanoic acid	74	20
gold/hexadecanethiol	99	29
gold/mercaptopropanesulfonic acid	68	19
gold/mercaptophenol	71	31
gold/mercaptopropanol	74	27

identical to those of the original urchin skeletal plates after 24 h of incubation time (Figure 2a), a result consistent with previously published data.[22,23] The single-crystal character of these particles is demonstrated by the presence of {104} faces at the peripheries of the particles, which lie parallel over the entire crystal. This is illustrated in Figure 2a, in which two different sets of {104} faces are noted with arrows. That this type of morphological analysis is a reliable measure of the single-crystal character of the templated particles has been confirmed by single-crystal diffraction of individual particles, as described in our previous work.[22−24] A single-crystal XRD pattern of a templated calcite particle produced as that shown in Figure 2a is additionally shown as an inset in this figure.

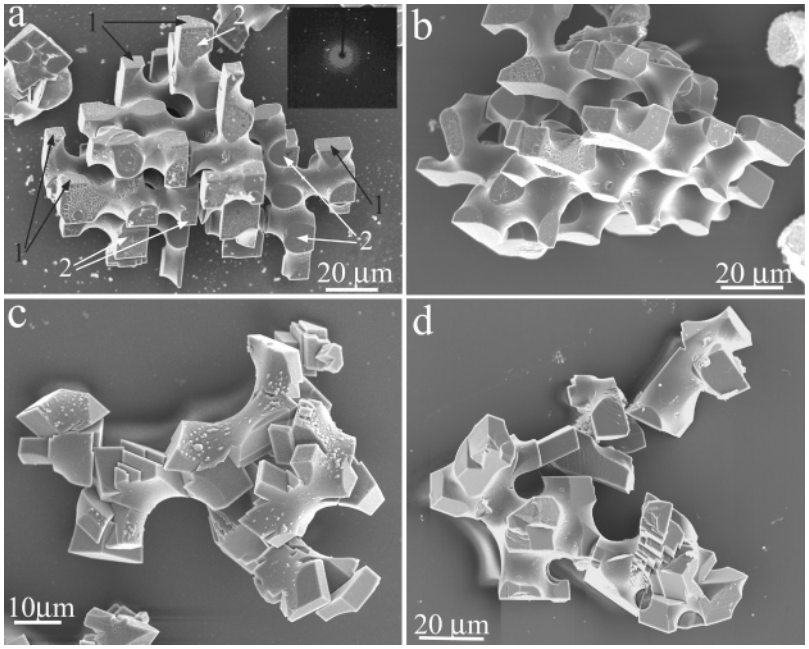

Figure 2. Calcite particles grown within surface-treated polymer membranes: (a) untreated membrane; (b) Au/hexadecanethiol-treated membrane; (c) Au/mercaptohexadecanoic acid-treated membrane; and (d) oxygen-plasma-treated membrane. The single-crystal nature of the particle shown in part a is demonstrated by the illustration of two different sets of parallel {104} faces present on the particle, labeled 1 and 2. The inset shows a single-crystal XRD pattern of a templated calcite particle produced under the same condition, confirming single-crystal character.

Growth of $CaCO_3$ within the gold-coated membrane yielded a similar result, producing single crystals of calcite with sponge-like structures. A slight increase in the percentage of vaterite particles was noted, with about 30% of particles being vaterite, as compared with 10−15% in the unmodified polymer membrane. Similarly, the positively charged membranes also supported the growth of templated calcite single crystals.

Functionalization of the gold-coated polymer membrane with a range of SAMs had a marked influence on the structure of the particles grown within the polymer membrane, according to the terminal group expressed by the monolayer. The Au/hexadecanethiol SAM offered the most hydrophobic environment and supported the growth of templated single crystals of calcite, 70−100 μm in size and identical in form to those produced in the untreated membranes (Figure 2b). After 24 h of incubation the population of particles isolated was approximately 70:30 calcite/vaterite. Both of the alcohol terminated SAMs, Au/mercaptophenol and Au/mercaptopropanol, also yielded templated, sponge-like calcite crystals which were of typical sizes 50 μm and 60−90 μm, respectively (data not shown). The proportion of vaterite particles observed in these systems varied from 10 to 30%.

The negatively charged SAMs (Au/mercaptohexadecanoic acid and Au/mercaptopropanesulfonic acid), in contrast, directed the formation of intergrown, polycrystalline calcite particles. These particles were 80−100 μm in size and were almost 100% calcite. The gross morphologies of the particles grown in these systems were sponge-like in form and clearly directed by the structure of the template (Figure 2c). However, while some curved surfaces were present, as would occur when the growth of a crystal is limited by contact with the polymer template, the particles principally comprise intergrown calcite rhombohedra of size $\sim$ 10 μm. Notably, these are randomly oriented over the volume of the particle, indicating that this particle did not originate from a single nucleation site. Polycrystalline particles also formed within the oxygen-plasma-treated polymer membranes (Figure 2d) and were similar in structure to those produced with the Au/negatively charged SAMs, showing evidence of templating and comprising intergrown rhombohedral calcite particles. The overall size of particles was $\sim$ 100 μm, and the ratio of calcite/vaterite was about 80:20.

The data therefore strongly suggested that the formation of large, templated single crystals within the membrane relied upon the presence of limited nucleation sites. The negatively charged membranes are anticipated to offer multiple nucleation sites and thus support the growth of polycrystalline particles. This observation was further studied by extending the investigation to the growth of $SrSO_4$ and $PbSO_4$ crystals within the surface-modified polymer membranes. Again, previous studies have shown that templated single crystals of $SrSO_4$ and $PbSO_4$ can be produced within untreated polymer membranes under appropriate experimental conditions.[24] Interestingly, precipitation of $SrSO_4$ from 0.05 M $SrCl_2$ and Na_2SO_4 and $PbSO_4$ from 0.02 M $Pb(NO_3)_2$ and Na_2SO_4 over 24 h resulted in single crystals for the untreated and all of the surface-treated membranes. In all of the membranes investigated, the $SrSO_4$ crystals typically grew to sizes of 100−130 μm and showed well-defined crystal faces which were parallel over the entire particles (Figure 3a). Similarly, templated single crystals of $PbSO_4$ with sizes of 60−80 μm were produced in all membranes (Figure 3b).

The membrane surface chemistry therefore appeared to exert little influence on the nucleation and growth of $SrSO_4$ and $PbSO_4$ within the membranes under the experimental conditions described. Analysis of the pH of the reagent solutions used for the precipitation of $CaCO_3$, $SrSO_4$, and $PbSO_4$ showed that $PbSO_4$ precipitated at pH 5.7, a signifi-

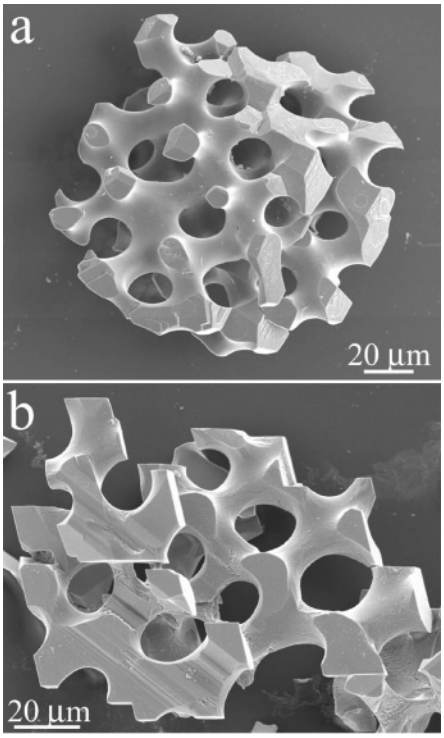

Figure 3. (a) $SrSO_4$ single crystal precipitated within a Au/ mercaptopropanesulfonic acid-treated polymer membrane and (b) a $PbSO_4$ single-crystal precipitated within a Au/mercaptohexadecanoic acid-treated membrane.

Table 2. pH Values of Reagent Solutions Used for the Precipitation of $CaCO_3$, $SrSO_4$, and $PbSO_4$ where pH(1) Is the Uncorrected pH Value and pH(2) is the Corrected pH Value

$CaCO_3$	pH	$SrSO_4$	pH(1)	pH(2)	$PbSO_4$	pH(1)	pH(2)
0.02 M $CaCl_2$	6.8	0.05 M $SrCl_2$	7.9	7.9	0.02 M $Pb(NO_3)_2$	4.7	6.1
0.02 M Na_2CO_3	10.7	0.05 M $Na_2(SO_4)$	7.8	11.5	0.02 M $Na_2(SO_4)$	8.0	12.6
pH after mixing	8.3		7.9	11.0		5.7	7.3

cantly lower pH value than that of $CaCO_3$ and $SrSO_4$, both of which precipitated at ~ pH 8 (Table 2). At higher pH values, ionization of the functional groups of the mercaptopropanesulfonic acid and mercaptohexadecanoic acid SAMs will occur, resulting in greater association of the Ca^{2+} and Sr^{2+} cations with the membrane surface and offering the possibility of a higher nucleation density on the membrane. The pH values of the reagent solutions were therefore adjusted to the values given in Table 2 prior to use to investigate the effect on the growth of $SrSO_4$ and $PbSO_4$ within the membranes. Modest increases in the pH of the $PbSO_4$ reagent solution to values greater than ~6.5 resulted in precipitation of $Pb(OH)_2$ as an initial phase, such that higher pH values could not be sensibly investigated in this system. At pH 11, templated single crystals of $SrSO_4$ 120−160 μm in size were principally produced (Figure 4a) in the oxygen-plasma-treated membranes and within the membranes functionalized with negatively charged SAMs (Au/mercaptohexadecanoic acid and Au/mercaptopropanesulfonic acid). Some templated particles comprising both single-crystal and polycrystalline $SrSO_4$ were also produced under these conditions (Figure 4b). Similar results were obtained within the untreated polymer membranes, indicating that the observation of some polycrystallinity reflected the change in pH as opposed to the influence of the membrane surface chemistry.

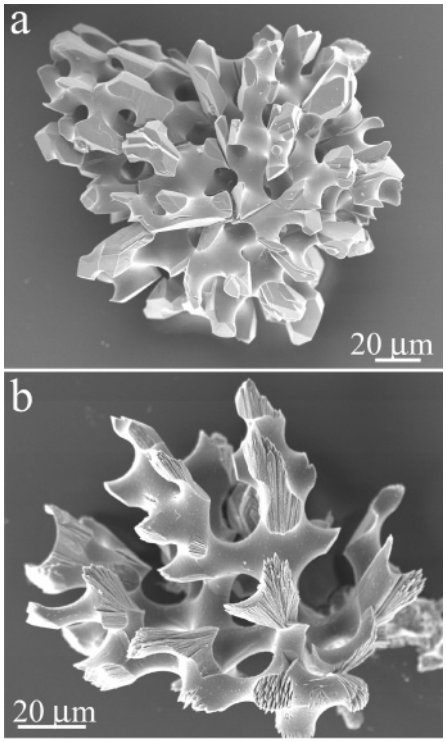

Figure 4. (a) $SrSO_4$ single crystal precipitated within a Au/mercaptopropanesulfonic acid-treated polymer membrane from 0.05 M $Na_2(SO_4)$, pH = 8.0, and 0.05 M $SrCl_2$, pH = 11.5, and (b) a $SrSO_4$ particle precipitated within a Au/mercaptohexadecanoic acid-treated membrane under the same experimental conditions showing mixed polycrystalline/ single-crystal structure.

Discussion

The formation of polycrystalline solids with large, complex structures via templating is reasonably straightforward, as evidenced by precipitation in systems as diverse as colloidal crystals,[41−43] bicontinuous microemulsions,[44] wood,[45] and commercial filtration membranes.[46] In contrast, the requirements for forming single crystals with elaborate morphologies appear far more stringent, and very few examples have been described in the literature. Possibly the most restrictive requirement for templating of single crystals is that the equilibrium size of the selected crystal must exceed the length scale of the template. In this respect calcite is a perfect—and indeed frequent—choice by organisms when they wish to produce large single crystals, as it readily grows to a micrometer length scale even under rapid precipitation conditions.

As supported by the data presented here, the growth of large single crystals is also dependent on the density of

(41) Geraud, E.; Prevot, V.; Ghanbaja, J.; Leroux, F. *Chem. Mater.* **2006**, *18*, 238−240.
(42) Sorensen, E. M.; Barry, S. J.; Jung, H. K.; Rondinelli, J. R.; Vaughey, J. T.; Poppelmeier, K. R. *Chem. Mater.* **2006**, *18*, 482−289.
(43) Sadakane, M.; Asanuma, T.; Kubo, J.; Ueda, W. *Chem. Mater.* **2005**, *17*, 3546−3551.
(44) Walsh, D.; Lebeau, B.; Mann, S. *Adv. Mater.* **1999**, *11*, 324−328.
(45) Zampieri, A.; Sieber, H.; Selvam, T.; Mabande, G. T. P.; Schwieger, W.; Scheffler, F.; Scheffler, M.; Greil, P. *Adv. Mater.* **2005**, *17*, 344−349.
(46) Schattka, J. H.; Wong, E. H. M.; Antonietti, M.; Caruso, R. A. *J. Mater. Chem.* **2006**, *16*, 1414−1420.

crystal nuclei formed in the system. Necessarily, a large single crystal must develop from a single nucleation site, indicating the presence of few nucleation sites in the system. In contrast, close-packed nuclei will grow until they impinge on each other, forming an intergrown polycrystalline solid. We have demonstrated that the nucleation of calcite in the polymer membranes can be controlled according to the membrane surface chemistry. While the native polymer membrane, positively charged membrane, and membranes functionalized with methyl- and hydroxy-terminated SAMs offer poor surfaces for the nucleation of calcite, the negatively charged plasma-treated membranes and membranes functionalized with carboxy- and sulfonate-terminated SAMs promote nucleation, resulting in the growth of polycrystalline solids.

Precipitation of $PbSO_4$ and $SrSO_4$ within the surface-treated membranes was also investigated, as formation of templated single crystals had successfully been achieved for both of these crystals within the untreated membranes.[24] Under the initial pH conditions of pH = 5.7, templated single crystals of $PbSO_4$ were produced in all of the surface-treated membranes. A modest increase in pH to 7.3 resulted in precipitation of $Pb(OH)_2$ as an initial phase, such that higher pH values could not be investigated in this system. Investigation of the effect of pH for the $SrSO_4$ also showed little effect of the membrane surface on the crystal nucleation process under the experimental conditions of $[Sr^{2+}] = 50$ mM and pH values of pH = 7.9 and 11.0.

That a surface effect was obtained for nucleation of the calcite crystals in the membrane but not for the $SrSO_4$ is intriguing. Experiments were carried out at similar pH values (8.3 for calcite and 7.9 for the $SrSO_4$) under which conditions the degree of ionization of the surface and interactions with the cations in solution would have been similar. Indeed, that epitaxial control of $CaCO_3$ nucleation by SAMs[30,32] and Langmuir monolayers[26,28,47] and SrF_2 by Langmuir monolayers[48] has been observed in this pH regime supports this argument. Heterogeneous nucleation on the substrate will depend on the interfacial energy between the crystal and the substrate and therefore also on the pK_a value of the substrate and the pH, because these will determine the degree of ionization of the substrate and therefore the interaction of the growing nucleus with the substrate at the experimental pH. Estimates of the pK_a values of the treated-membrane surfaces can be suggested based on literature values. Undecyl-sulfonate and siloxane anchored SAMs have been quoted as exhibiting pK_a values of 2 and showing complete deprotonation above ~pH 5,[49] while pK_a values quoted for carboxylic acid terminated thiol SAMs on gold have ranged from 5.2 to 11.5, according to the chain length, substrate roughness, and ionic strength (ref 50 and references therein). Measured values for rough substrates, which are most consistent with the current experiments, have varied from 5.4 to 6.3.[50] In the case of long-chain carboxylate terminated silane monolayers, pK_a values in excess of 5.4 have been measured, and deprotonation levels of 30%, 85%, and 100% have been determined at pH values of 7, 9, and 11, respectively.[51] Therefore, the polymer surfaces functionalized with the carboxylic and sulfonic acid groups would have been strongly negatively charged for the experiments carried out at pH ~ 7 and above, resulting in binding of the Ca^{2+} and Sr^{2+} cations from solution.

The control of crystal nucleation by the membrane surface in our system can be broadly considered in terms of classical nucleation theory.[52−54] Liu and Lim considered the problem of heterogeneous nucleation on foreign particles of varying radii and contact angles between the substrate and nucleating crystal and demonstrated that foreign particles with lower contact angles/larger radii would dominate at low supersaturations, while nucleation on particles with larger contact angles and smaller radii would become kinetically favorable at high supersaturations.[55,56] Under very high supersaturation conditions, homogeneous nucleation will predominate. A rough estimation of the initial supersaturation conditions in our experiments was undertaken on the basis of starting solution concentrations and pH with the program PHRQPITZ, using Pitzer equations to determine activity coefficients. Values of K_{sp} of $10^{-8.43}$ for calcite[57] and $10^{-6.5}$ for $SrSO_4$[58] were applied. These calculations are intended to provide a ballpark figure only, as experiments were carried out under double diffusion conditions, such that the solution concentrations when nucleation occurred are not readily determined. Concentration limits based on non-dilution of initial reagent concentrations and complete solution mixing were therefore evaluated. For calcite, the supersaturation ratio $S = IAP/K_{sp}$ where IAP is the ion activity product was calculated to lie between $S = 268$ and $S = 80$ (calculated for 20 mM and 10 mM initial reagents concentrations, respectively), with an initial driving force for crystallization $(\Delta\mu/k_BT) = \ln S = 5.59$ for 20 mM reagents and $\ln S = 4.38$ for 10 mM reagents. For $SrSO_4$, S was calculated to lie between $S = 285$ and $S = 131$ for 50 mM and 25 mM initial reagent concentrations at pH 7.9 and $S = 284$ and $S = 131$ for 50 mM reagents and 25 mM reagents at pH 11.

These rough calculations demonstrate that precipitation of both $CaCO_3$ and $SrSO_4$ occurred under very high supersaturation conditions, far exceeding values where a transition from heterogeneous to homogeneous nucleation would be predicted. Stopped flow precipitation data for $CaCO_3$ have indicated a change from heterogeneous to homogeneous

(47) Donners, J. J. J. M.; Nolte, R. J. M.; Sommerdijk, N. A. J. M. *J. Am. Chem. Soc.* **2002**, *124*, 9700−9701.
(48) Kmetko, J.; Yu, C.; Evmenenko, G.; Kewalramani, S.; Dutta, P. *Phys. Rev. B* **2003**, *68*, 085415−085411.
(49) Shyue, J. J.; DeGuire, M. R.; Nakanishi, T.; Masuda, Y.; Koumoto, K.; Sukenik, C. N. *Langmuir* **2004**, *20*, 8693−8698.
(50) Leopold, M. C.; Black, J. A.; Bowden, E. F. *Langmuir* **2002**, *18*, 978−980.
(51) Cheng, S. S.; Scherson, D. A.; Sukenik, C. N. *Langmuir* **1995**, *11*, 1190−1195.
(52) Mullin, J. W. *Crystallization*, 3rd ed.; Butterworth-Heinemann: Oxford, 1993.
(53) Wu, W.; Nancollas, G. H. *Adv. Colloid Interface Sci.* **1999**, *79*, 229−279.
(54) DeYoreo, J. J.; Vekilov, P. G. *Rev. Mineral. Geochem.* **2003**, *54*, 57−93.
(55) Liu, X. Y. *J. Cryst. Growth* **2002**, *237−239*, 1806−1812.
(56) Liu, X. Y.; Lim, S. W. *J. Am. Chem. Soc.* **2003**, *125*, 888−895.
(57) Wijden, R. D. v. d.; Hiejden, A. E. v. d.; Witkamp, G. J.; Rosmalen, G. M. v. *J. Cryst. Growth* **1997**, *171*, 190−196.
(58) Malollari, I. X.; Klepetsanis, P. G.; Koutsoukos, P. G. *J. Cryst. Growth* **1995**, *155*, 240−246.

nucleation at $S \sim 20$,[59] while it has been proposed that homogeneous nucleation proceeds for $SrSO_4$ at values of $S > 8$.[58] Travaille et al. combined experimental measurements with classical heterogeneous nucleation theory to consider the nucleation of calcite on carboxylic acid terminated SAMs and observed nucleation in solution at $\Delta\mu/k_BT > 4.84$ and $S > 126$ and epitaxial nucleation of calcite on the substrate in addition to precipitation in solution at driving forces $\Delta\mu/k_BT > 5.1$ and $S > 164$.[60] Nucleation under all conditions was classified as heterogeneous in character, as calcite crystals grew epitaxially on the substrate demonstrating direct control of the nucleation process by the substrate, and it was considered unreasonable that homogeneous nucleation would occur at lower supersaturations than heterogeneous. Differences in the crystal nucleation behavior of $CaCO_3$ and $SrSO_4$ may derive from variations in the crystal/solution and crystal/substrate interfacial energies, as well as from differences in the supersaturation levels. Literature values of the crystal/solution interfacial energies of calcite and $SrSO_4$ are however broadly similar, with values of 68−97 mJ m^{-2} being commonly reported for calcite[53,60−62] and 62−103 mJ m^{-2} reported for $SrSO_4$,[58,61,63,64] depending on the solution composition and measurement methodology applied.

Although consideration of the $CaCO_3$ and $SrSO_4$ systems shows that crystallization occurred under similar solution conditions, one significant difference does exist between these crystals—the rich polymorphism exhibited by $CaCO_3$. Under the reaction conditions employed here, initial precipitation of ACC would be anticipated.[65−68] The ACC will be short-lived, rapidly redissolve, and reprecipitate as the stable calcite phase. Therefore, the first phase formed at a charged membrane surface may be ACC, which could either occur via heterogeneous nucleation or through adsorption of particles formed by homogeneous nucleation in solution. Indeed, our previous work on $CaCO_3$ precipitation in the untreated polymer membranes from 0.02 M reagents showed that double-sided templated particles formed as a sheet of $CaCO_3$ of the membrane surface were present in addition to solid templated calcite and vaterite particles at early times.[22] These short-lived particles were considered to form via an ACC precursor phase. Control experiments, in which 0.02 M reagents were combined in bulk solution, also showed that ACC was the first phase formed under these conditions.

That ACC was formed within the membrane at early incubation times was supported in the current work by analysis of the membrane after 15 min. Imaging of the membrane with SEM clearly showed the presence of ACC particles in addition to a small number of nascent calcite crystals, as identified by their roughly spherical morphologies, either coating the membrane surface (Figure 5) or in the pore volume. Raman microscopy of the dried membranes isolated after the same time also supported the conclusion that the particles were ACC but did not provide conclusive evidence. The spectra of the membranes showed no additional peaks attributable to $CaCO_3$, demonstrating either that the particles identified by SEM were ACC or that they were present in too low quantities as compared with the membrane support to be characterized. At wavenumbers above ~300 cm^{-1}, which were accessible here with the 488 nm Ar ion laser, calcite displays a weak band at 712 cm^{-1} and strong sharp band at 1085 cm^{-1}, while ACC shows a broader and weaker band at 1085 cm^{-1} and no detectable peak at 712 cm^{-1}.[37,69−71] Unfortunately, analysis of the membrane itself showed strong peaks in the 1100 cm^{-1} region which would effectively mask the relatively weak 1085 cm^{-1} band of ACC, while had the particles been principally calcite, the stronger calcite band in the same position would have still been visible. Therefore, no additional peaks at either 712 cm^{-1} (unmasked by the membrane spectrum) or 1085 cm^{-1} suggests that the particles produced are either predominantly ACC or that they are present in too low concentrations to be analyzed.

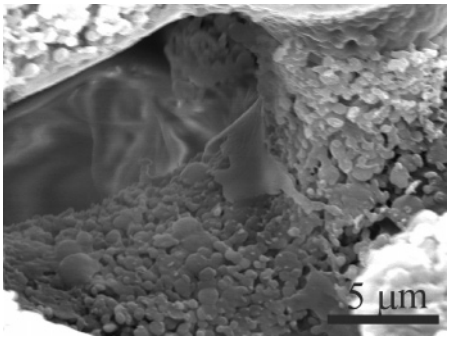

Figure 5. SEM image of the surface of an untreated membrane in which $CaCO_3$ has been precipitated, isolated after 15 min from the double diffusion setup.

These results therefore combine to strongly indicate the presence of ACC as a transient precursor phase in this system. The ACC precursor phase will generate a high density of Ca^{2+} and CO_3^{2-} ions at the membrane/solution interface, and subsequent recrystallization will be directed by the membrane. Stabilization of ACC through interaction with organic molecules has been demonstrated on many occasions using small molecules,[72] polymers,[73] and organic aggregates.[74] That an organic substrate can also exert control over the nucleation of a crystalline $CaCO_3$ product from an

(59) Sohnel, O.; Mullin, J. W. *J. Cryst. Growth* **1978**, *44*, 377−382.
(60) Travaille, A. M.; Steijven, E. G. A.; Meekes, H.; Kempen, H. v. *J. Phys. Chem. B* **2005**, *109*, 5618−5626.
(61) Bennema, P.; Sohnel, O. *J. Cryst. Growth* **1990**, *102*, 547−556.
(62) Koutsoukos, P. G.; Kontoyannis, C. G. *J. Chem. Soc., Farady Trans. I* **1984**, *80*, 1181−1192.
(63) He, S.; Oddo, J. E.; Tomson, M. B. *J. Colloid Interface Sci.* **1995**, *174*, 327−335.
(64) Hina, A.; Nancollas, G. H. *Rev. Mineral. Geochem.* **2000**, *40*, 277−301.
(65) Clarkson, J. R.; Price, T. J.; Adams, C. J. *J. Chem. Soc., Faraday Trans.* **1992**, *88*, 243−249.
(66) Ogino, T.; Suzuki, T.; Sawada, K. *Geochim. Cosmochim. Acta* **1987**, *51*, 2757−2767.
(67) Bolze, J.; Peng, B.; Dingenouts, N.; Panine, P.; Narayanan, T.; Ballauff, M. *Langmuir* **2002**, *18*, 8364−8369.
(68) Brecevic, L.; Nielsen, A. E. *J. Cryst. Growth* **1989**, *98*, 504−510.
(69) Weiner, S.; Levi-Kalisman, Y.; Raz, S.; Addadi, L. *Connect. Tissue Res.* **2003**, *44*, 214−218.
(70) Behrens, G.; Kuhn, L. T.; Ubic, R.; Heuer, A. H. *Spectrosc. Lett.* **1995**, *28*, 983−995.
(71) Edwards, H. G. M.; Villar, S. E. J.; Jehlicka, J.; Munshi, T. *Spectrochim. Acta, Part A* **2005**, *61*, 2273−2280.
(72) Xu, A.-W.; Yi, Q.; Dong, W.-F.; Antonietti, M.; Colfen, H. *Adv. Mater.* **2005**, *17*, 2217−2221.
(73) Guillemet, B.; Faatz, M.; Grohn, F.; Wegner, G.; Gnanou, Y. *Langmuir* **2006**, *22*, 1875−1879.
(74) Donners, J. J. J. M.; Heywood, B. R.; Meijer, E. W.; Nolte, R. J. M.; Sommerdijk, N. A. J. M. *Chem.—Eur. J.* **1992**, *8*, 2561−2567.

ACC precursor phase was unambiguously demonstrated by the formation of oriented calcite thin films under Langmuir monolayers of porphyrin amphiphiles, via an ACC precursor phase.[75]

We therefore suggest that all of our experiments were carried out under supersaturation conditions where the membrane does not significantly promote nucleation. This is apparent in the $SrSO_4$ system where similar single-crystal products were produced in all membranes, independent of their surface treatment. In contrast, a strong surface dependence was observed for the calcite system, which is attributed to the formation of an amorphous precursor phase. The ACC phase is intimately associated with the membrane and mediates the recrystallization process, resulting in multiple nucleation sites and a polycrystalline product when ionizable surface groups are present. Future work will clarify the role of the solution supersaturation and the presence of an ACC precursor phase by examining the role of surface mediated control of nucleation under varying experimental conditions. This is not easily achieved within our current system as only a very small number of particles are precipitated within the membranes at low solution concentrations, and these are then difficult to isolate.

Conclusions

Our experiments have shown that the formation of single crystals with complex morphologies by a templating route is uniquely determined by the solution conditions and the surface chemistry of the template. Under relatively high supersaturation conditions and pH levels where significant ionization of the polymer membrane surface groups occurs, single crystals of $SrSO_4$ formed in all the polymer membranes investigated. This result is consistent with an anticipated reduced influence of the membrane surface at high supersaturation conditions. In contrast, a strong dependence of the single-crystal/polycrystalline structure of the product calcite particles on the membrane surface chemistry was observed under equivalent reaction conditions. Here, the surface dependence of calcite nucleation was attributed to the formation of a precursor ACC phase. Calcium carbonate therefore seems to offer a uniquely flexible mineral system where control over nucleation and, therefore, fundamental properties of the product phase including polycrystallinity and polymorph can be exerted over a wide range of reaction conditions.

Acknowledgment. Financial support from the Engineering and Physical Sciences Research Council (EPSRC, Grant GR/S79732/01) is gratefully acknowledged.

CM0620640

(75) Gu, G. F.; Yao, N.; Aksay, I. A.; Groves, J. T. *J. Am. Chem. Soc.* **1998**, *120*, 11977.